AN OVERVIEW OF DEFECTIVE FUEL ANALYSIS IN CANDU AND LIGHT WATER REACTORS

B.J. Lewis
Royal Military College of Canada, P.O. Box 17000, Kingston, Ontario, CANADA K7K 7B4

ABSTRACT

The theory used in various defective-fuel monitoring packages for both CANDU and Light Water Reactors is reviewed. A fuel-oxidation model is proposed for operating defective fuel rods to account for high-pressure and radiolysis effects. Based on the results of the fuel oxidation model, a correlation is proposed to predict the power of the defective rods from the measured coolant activity at two different power levels of the reactor.

1. INTRODUCTION

Several methodologies have been developed over the past number of years for the in-core characterization of defective fuel rods during normal reactor operation based on a coolant activity analysis in both CANDU and Light Water Reactors.[1-8] For instance, the isotopic activities of the more volatile noble gas, iodine and cesium products in the reactor coolant system (RCS) can provide a prediction of the number of fuel failures, a characterization of the defect state (e.g., size and location), the defective fuel rod power and burnup, and the amount of tramp uranium that has deposited on the in-core surfaces. A review of the current theory used in the various analysis tools for defective fuel monitoring is presented.

The release behaviour of fission products from defective rods will depend directly on the fuel oxidation state. More mechanistic theoretical treatments are currently being developed to predict the fuel oxidation kinetics at high pressure during normal defect operation.[9,10] Fuel oxidation will occur with the presence of steam in the fuel-to-clad gap due to coolant entry through the defect site. In addition, fuel oxidation may also result from reaction with highly-reactive hydrogen peroxide produced in the gap due to radiolysis of steam by fission-fragment bombardment.[11-13] A theoretical treatment for describing the fuel oxidation kinetics in operating defective rods is discussed in the paper. Furthermore, based on in-reactor experiments and mechanistic modelling, a correlation is proposed for CANDU fuel to determine the average power of the defective rods based on the measured coolant activity by considering the effects of fuel oxidation.

2. DEFECTIVE FUEL ANALYSIS PACKAGES

A number of analytical tools have been developed to characterize defective fuel rods based on on-line coolant activity analysis. For example, analysis packages have been developed for the French Pressurized Water Reactor (PWR) by the Commissariat à l'Energie Atomique (CEA) and Electricité de France (EdF) which include the PROFIP and SADDAM computer codes.[1,3] For Boiling Water Reactor (BWR) and PWR analyses in the United States, the Battelle Pacific Northwest Laboratories have developed the industry-standard American Nuclear Society (ANS 5.3) model.[4] This model, in turn, has evolved into the CHIRON computer code, developed under the sponsorship of the Electric Power Research Institute (EPRI), for use by the utility members of EPRI. The ANS 5.3 model in fact has similar theoretical underpinning to the earlier developed and still evolving CADE code, which is used for vendor analysis at the Westinghouse Electric Corporation.[5] The Tawain Power Company has also used the ANS 5.3 methodology in the development of the FREM model for BWR applications.[6] For CANDU reactor analysis, a physically-based model has been developed at the Royal Military College (RMC), employing an expert system architecture, using release data obtained from in-reactor loop experiments at the Chalk River Laboratories (CRL).[7] In the United Kingdom, Nuclear Electric have also developed the BTC model, for steady-state coolant activity analysis of noble gases and iodine, as well as for transient iodine-spike analysis, for use in reactor management of failed fuel in PWRs.[8] The BTC model is based on a similar theoretical treatment as for the ANS 5.3 and CANDU models (using first order kinetic theory to describe the fission product transport in the gap), and also makes use of the CRL in-reactor data.

2.1 *Fission Product Release Theory*

The model in the various analysis packages for describing fission product release from defective fuel rods is typically based on the theory of solid-state diffusional transport in the fuel matrix, and diffusional or first-order kinetic transport in the fuel-to-clad gap.

For n defect sites located symmetrically along the rod (see Fig. 1), the axial-transport equation for the steady-state diffusion of radioactive fission products in the gap toward the defect site is:[14]

$$D\frac{d^2C}{dx^2} - \lambda C + \frac{R_f}{l} = 0, \tag{1}$$

where C is the fission product distribution per unit length in the gap, λ is the decay constant, D is the gap diffusion coefficient and R_f is the fission product release rate from the fuel into the gap of length l. Equation (1) is subject to two boundary conditions: (i) a reflexive condition at both ends of the rod and at the various mid-point locations between any two defect sites:

$$\frac{dC}{dx} = 0, \tag{2a}$$

and (ii) a surface-exchange condition at the cladding failure site(s)

$$D\frac{dC}{dx} = \alpha(C - C_c) \approx \alpha C. \tag{2b}$$

Here α is a surface-exchange coefficient, and C_c is the bulk fission-product concentration in the coolant (where normally $C_c << C$). For a diffusional release from the fuel matrix:

$$R_f = 3\sqrt{\frac{D'}{\lambda}}B \tag{3}$$

where D' is the effective fission-product diffusivity in the fuel matrix and B is the fission product birth rate. Thus, solving Eq. (1) subject to the given boundary conditions, and employing the Fick's first law of diffusion, the general expression for describing the (steady-state) release rate of volatile fission products into the RCS is given by[14]

$$R_c = \left(\frac{2nL}{l}\right)\alpha\left(\frac{\tanh\left(\frac{l}{2nL}\right)}{\frac{D}{L}\tanh\left(\frac{l}{2nL}\right) + \alpha}\right)R_f, \tag{4}$$

where the diffusion length $L = (D/\lambda)^{1/2}$. If the cladding defect offers little holdup compared to the axial path length along the fuel-to-clad gap, then $\alpha >> (D/L)\tanh(l/2nL)$, and diffusion becomes the rate-limiting step for the migration of fission products in the gap. In this case, Eqs. (3) and (4) yield so the so-called diffusion model for gap transport:[11]

$$\frac{R_c}{B} = \left(\frac{2nL}{l}\right)\tanh\left(\frac{l}{2nL}\right)3\sqrt{\frac{D'}{\lambda}}. \tag{5a}$$

On the other hand, if the diffusion length is much greater than the axial path length for release, i.e., $L >> l/2n$, then $\tanh(l/2nL) \approx (l/2nL)$, and Eq. (4) reduces to:

$$\frac{R_c}{B} = \left(\frac{\varepsilon}{\lambda + \varepsilon}\right)3\sqrt{\frac{D'}{\lambda}}, \tag{5b}$$

where

$$\varepsilon = (2n\alpha)/l. \tag{5c}$$

Note that in the derivation of Eq. (5c), it follows that $n = ½$ for an end-rod defect and $n = 1$ for a single mid-rod defect. The gap escape rate coefficient, ε, can also be thought of as an effective transport velocity (α) for release, normalized over the axial path length ($l/2n$). The relation in Eq. (5b) is normally termed a first-order kinetic model. In particular, this model can also be derived by assuming a first-order rate process where R_c is proportional to the inventory in the gap, with a proportionality constant ε. However, the specific relation in Eq. (5c) does not follow with this latter approach. Equation (5b) is used as the standard model of release from defective fuel rods for the various analysis packages in Refs. 1 through 8.

Fission product release from tramp uranium deposited on in-core reactor surfaces can be distinguished from that of defective rods since the predominant release mechanism is low-temperature recoil. In this case, the (R_c/B) ratio is given by[15]

$$\frac{R_c}{B} = \frac{1}{2}\left[\frac{1}{\alpha^3} + \frac{3r}{2d}\left(1 - \frac{1}{\alpha^2}\right)\right] \approx \frac{1}{2}, \tag{6}$$

where $\alpha = \max(1, d/r)$. Since the diameter of the fuel particle d (~ 7 µm) is approximately equal to the range of the fission fragment r (~ 8 µm) (see Fig. 2), α is therefore equal to unity. Thus, the (R_c/B) ratio reduces to a constant value of ½ that is independent of λ (in contrast to Eq. (5b)).

Hence, in the various analysis packages, the fission product release from the defective fuel rods is distinguished from the tramp uranium release by combining Eqs. (5b) and (6) which leads to the correlational relationship:

$$\left(\frac{R}{B}\right)_{meas} = \left(\frac{A_i}{FY_i\lambda_i}\right) = \underbrace{\left(\frac{\varepsilon}{\varepsilon+\lambda}\right)\frac{a}{\sqrt{\lambda}}}_{Defective\ Rods} + \underbrace{c}_{Tramp\ U} \tag{7}$$

Here F is the average fission rate in the core and Y_i is the fission yield of fission product i. The parameters ε, a and c are obtained with a fitting of Eq. (7) to the measured coolant activities (A_i). For a BWR, A_i is the measured off gas activity (in Bq/s), whereas for a PWR or CANDU, $A_i = M_i V_c(\lambda_i + \beta)$ where M_i is the measured coolant activity concentration (in Bq m^{-3}) and V_c is the reactor coolant system (RCS) volume.[4,7] The latter relation accounts for coolant purification (i.e., ion exchange cleanup of radioiodine) with a rate constant β. An example of this type of methodology for the off gas analysis of a BWR plant is shown in Fig. 3.

Based on a fitting of Eq. (7) to the measured coolant activity, the amount of tramp uranium can be determined from the fitted value of c as previously detailed in Refs. 7 and 11. On the other hand, the fuel failures can be characterized from the fitted values of ε and a. A comparison of the different methodologies for fuel characterization for the various reactor types is given in Section 2.2.

2.2 *Fuel Failure Characterization*

The fuel monitoring packages provide such information as: (i) the number of defective rods; (ii) the size and location of defects; and (iii) the average burnup and power of the defective rods. This information is provided by comparison of the fitted parameters to that established from previous experience where the fuel rod conditions are well known. The various correlations for this type of analysis for LWR and CANDU fuel are summarized as follows.

(i) *Number of Defective Rods.* Since Eq. (7) actually applies to x defective rods, it follows that:

$$x = \frac{a}{3\sqrt{D_s'}} \tag{8}$$

where D_s' (in s^{-1}) is for a single defective rod. Correlations for the single-rod diffusivities for iodine (I) and noble gas (NG) for the different types of reactors are detailed in Table 1.

Table 1: Single-Rod Diffusivities

Analysis Package	Rector Type	Correlation for D_s' (s^{-1})$^{(a)}$
ANS 5.3	PWR	$D_I' = \begin{cases} 142.9\varepsilon^{2.26} & \varepsilon \leq 3.6\times10^{-6} \\ 7.11\times10^{-11} & \varepsilon \geq 3.6\times10^{-6} \end{cases}$
	BWR	$D_{NG}' = \begin{cases} 5.93\times10^{-11} & \varepsilon \leq 4\times10^{-5} \\ 2.09\times10^{9}\varepsilon^{4.44} & 4\times10^{-5} < \varepsilon < 8\times10^{-5} \\ 1.29\times10^{-9} & \varepsilon \geq 8\times10^{-5} \end{cases}$
RMC	CANDU	$\left.\begin{array}{l} D_I' = 10^{9.857\log P(kW/m) - 25.1314} \\ D_{NG}' = 10^{8.632\log P(kW/m) - 23.4091} \end{array}\right\} \quad 25 \leq P \leq 60$

(a) Taken from Refs. 4 and 7.

In the ANS 5.3 model, it is assumed for the lower-powered LWR fuel that D_s' (in s^{-1}) is only dependent on ε (in s^{-1}).[4] Here it is argued that a larger value of the gap escape rate coefficient, ε, implies a larger defect size which will consequently lead to a greater amount of fuel oxidation. This effect, in turn, results in an enhanced fission-product diffusivity, D_s', in the fuel matrix. On the other hand, in the RMC model, for the higher-powered CANDU fuel, it is implicitly assumed that D_s' correlates with only the fuel rod linear power, P (in kW/m), based on the results of the CRL experiments.[7] In comparison, in the SADDAM model for PWR fuel, Eq. (7) is simplified somewhat although it effectively covers the same exponential dependence on λ as results in Eq. (7):[3]

$$\left(\frac{R}{B}\right)_{meas} \approx k\lambda^{-n}, \quad \text{where } 0.35 < n < 0.7. \tag{9}$$

Thus, fitting Eq. (9) to the coolant activity data and normalizing the model prediction for Xe-133 by the single-rod value yields:

$$x = \left(\frac{R}{B}\right)_{Xe-133} \Big/ \left(\frac{R}{B}\right)^{s}_{Xe-133} \quad \text{where } \left(\frac{R}{B}\right)^{s}_{Xe-133} = 0.01. \tag{10}$$

The two methodologies in Eqs. (8) and (10) are essentially equivalent.

(ii) *Defect Size and Location.* Although D_s' is given as a function of ε in Table 1 for the ANS 5.3 model, no further information is given about the defect size or location. In the RMC model, the defect location is first estimated in terms of the number of defect planes (for the given one-dimensional model in Fig. 1). This calculation is determined in accordance with Eq. (5c) using the value of ε_{NG}^{meas} obtained from the fitting to the noble gas coolant activity data:

$$n = \frac{\varepsilon_{NG}^{meas}\, l}{2\alpha_{NG}}. \tag{11}$$

The surface exchange coefficient α_{NG} has been previously determined from the CRL experiments and is constant for the chemically inert noble gas species, i.e., $\alpha_{NG} = 7.14 \times 10^{-6}$ m s^{-1}.[7] On the other hand, the iodine release is observed to strongly depend on the defect size, compared to that of the noble gases, since the iodine is chemically trapped on the internal fuel and clad surfaces. Iodine is therefore only released locally around the defect site where it is more soluble as the liquid coolant comes in contact with the gap atmosphere in this boundary region. Thus, with knowledge of n and the fitted value of ε_I^{meas} for the measured iodine activity in the coolant, the defect size E (in mm^2) can be evaluated from the correlation:[7]

$$\alpha_I(E) = \frac{\varepsilon_I^{meas} l}{2n} = 10^{0.7064 \log E(mm^2) - 7.5173} . \tag{12}$$

The second relation in Eq. (12) is again obtained from the CRL experiments.

As shown in Fig. 4, a similar analysis is also considered in the SADDAM model where the *(R/B)* ratio of a long-lived iodine isotope is compared to a noble gas one in order to exploit the chemical difference between these two species.[3]

(iii) *Burnup of Leaking Rods*. The average burnup of the leaking rods can be obtained from the ratio of ^{134}Cs/^{137}Cs activity measured in the coolant during power reactor transients. The long-lived ^{137}Cs (30.17 y half-life) is produced directly in the fission process and from the subsequent decay of its precursor products. However, ^{134}Cs (2.065 y half-life) is shielded in the β decay chain (by the stable isotope ^{134}Xe) and can therefore only be produced by neutron activation of ^{133}Cs with time (i.e., burnup). Since the ^{134}Cs/^{137}Cs activity ratio in the coolant is directly proportional to that in the uranium dioxide fuel, the fuel burnup can be determined by calculating the ratio (as a function of burnup) with a fission product accumulation code (e.g., ORIGEN) (see Fig. 5).[3,4]

This technique is less useful for CANDU fuel, than for the much higher-burnup LWR fuel, because of the limited cesium release at low burnup.

(iv) *Power of Leaking Rods*. The average power of the leaking rods is obtained in the SADDAM code by a correlation of the release-to-birth rate ratio versus the rod power.[2] In particular, the $(R/B)_{meas}$ ratio of ^{133}Xe is used to obtain the power fraction (P/P_n) in Fig. 6 and, with knowledge of the average linear rod power in the core P_n, the linear power of the defective rod(s) P is thus obtained. In Fig. 6, the gas release decreases when the cladding defect occurs later during the irradiation cycles. This correlation is possible since the fission product release from the fuel matrix is an Arrhenius function of temperature due to the mechanism of solid-state diffusion (see Eq. (5b)), which results in an increasing *(R/B)* ratio as a function of the fuel rod power. For instance, Fig. 7 shows the exponential behaviour of the empirical diffusivity for xenon observed as a function of the fuel rod power for CANDU-type fuel in the CRL sweep gas experiments (i.e., with unoxidizd fuel).[7,16]

A similar type of correlation to determine the average power of the leaking rods can be obtained for defective CANDU fuel by accounting for fuel oxidation effects as considered in Section 3. The correlation is proposed in Section 4.

3. FISSION PRODUCT DIFFUSIVITY AND FUEL OXIDATION

3.1 *Fission Product Diffusivity*

Fuel oxidation in defective rods will lead to an enhanced diffusion coefficient from that shown in Fig. 7. The derivation of the composite diffusion coefficient for stoichiometric and hyperstoichiometric fuel is given in Sections 3.1.1 and 3.1.2, respectively.

3.1.1 *Stoichiometric Fuel*

Measurements of release for rare gas fission products from single and polycrystalline uranium dioxide during irradiation at 800 to 1400°C were carried out at the Atomic Energy Research Establishment at Harwell. From these measurements, it was concluded that the diffusion coefficient was the sum of three separate components:[17,18,19]

(i) *Intrinsic Diffusion at High Temperature*. The intrinsic behaviour of the diffusion coefficient (in $m^2 s^{-1}$) at high temperature T (in K) was based on the results of Davies and Long:[20]

$$D_1(T) = 7.6 \times 10^{-10} \exp\left\{-\frac{70000}{RT}\right\} \tag{13}$$

where R (=1.987 cal mol^{-1} K^{-1}) is the ideal gas constant.

(ii) *Vacancy-Assisted Diffusion at Intermediate Temperature.* For the intermediate range of temperatures, the gas atom mobility is influenced by cation vacancies on adjacent lattice sites. During irradiation, the vacancy concentration can be enhanced as a result of irradiation damage. The concentration of irradiation-induced vacancies will be determined by mutual recombination at low temperatures and by diffusion to fixed sinks at high temperature. From the analysis of Sharp, the irradiation-induced vacancy concentration V is given by:[21]

$$V = \frac{\left(\alpha_s s^2 + Z_s V_o\right)}{2Z_s}\left\{\sqrt{1 + \frac{4KZ_s}{j_v\left(\alpha_s s^2 + Z_s V_o\right)^2}} - 1\right\} \tag{14}$$

where $V_o \sim \exp\{-5.52 \times 10^4/(RT)\}$ is the thermodynamic concentration (vacancies/atom), $\alpha_s \sim 10^{15}$ m^{-2} is the fixed sink strength, $s^2 \approx 10^{-19}$ m^2 is the square of the atomic jump distance, $Z_s \sim 100$ is the number of sites around a point defect from which recombination is inevitable, and $j_v = 10^{13} \exp\{-5.52 \times 10^4/(RT)\}$ s^{-1} is the vacancy jump rate. In the Harwell irradiation experiments, the rate of defect production per atom was evaluated as $K \approx 2 \times 10^{-4}$ defect s^{-1} atom^{-1} that corresponded to a damage rate of 5×10^5 defect s^{-1} fission^{-1}. The contribution of irradiation-produced vacancies to the composite diffusion coefficient, however, occurs in a temperature region where mutual recombination dominates. In this case, Eq. (14) simplifies to:[17]

$$V = \sqrt{\frac{K}{j_v Z_s}}. \tag{15}$$

The approximation of Eq. (15) explicitly results from Eq. (14) under the conditions that $\alpha_s s^2 >> Z_s V_o$ and $\{4KZ_s/j_v\}^{1/2} >> \alpha_s s^2$, which are valid at intermediate temperatures that are approximately ≤ 1500 K. Using Eq. (15), the gas diffusion coefficient in this regime will have the form:

$$D_2 \cong s^2 j_v V. \tag{16}$$

Since, the value of K ($\approx 2 \times 10^{-4}$ defect s^{-1} atom^{-1}) pertains to a fission rate density of $\dot{F} = 10^{19}$ fission m^{-3} s^{-1} in the Harwell experiments, D_2 (in m^2 s^{-1}) of Eq. (16) can be evaluated as a function of $\dot{F}$ (in fission m^{-3} s^{-1}) and temperature T (in K):

$$D_2 = \sqrt{2} \times 10^{-25} \sqrt{\dot{F}} \exp\left\{-\frac{2.76 \times 10^4}{RT}\right\}. \tag{17}$$

(iii) *Athermal Diffusion at Low Temperature.* For the low temperature component, Matzke showed in self-diffusion studies that that the athermal component was proportional to the fission rate density,[22] i.e., a fitting of this type of expression to the low-temperature Harwell gas results yielded the diffusivity (in m^2 s^{-1}) as a function of $\dot{F}$ (in fission m^{-3} s^{-1}):[17]

$$D_3 = 2 \times 10^{-40} \dot{F}. \tag{18}$$

In a more recent analysis of the data where recoil effects were considered, it was suggested that the intermediate (Eq. (17)) and athermal (Eq. (18)) components should be multiplied by a factor of 4.[18] Thus, the composite expression for the diffusion coefficient D (in m^2 s^{-1}) over the whole temperature range of interest is given by:

$$D(T,\dot{F}) = 7.6 \times 10^{-10} \exp\left\{-\frac{70000}{RT}\right\} + 4\left[\sqrt{2} \times 10^{-25} \sqrt{\dot{F}} \exp\left\{-\frac{27600}{RT}\right\} + 2 \times 10^{-40} \dot{F}\right]. \tag{19}$$

Equation (19) was also adopted in the FREEDOM fission product release code for unoxidized fuel conditions, where the same diffusion coefficient was assumed for the Kr, Xe, I and Cs species.[23] The FREEDOM fission product release model (and hence the on-power, stoichiometric diffusion coefficient) has been validated against the results of the CRL sweep gas experiments (i.e., FIO-122, FIO-124, FIO-133, FIO-134 and FIO-141), and the ELESIM database of fission gas release from commercial and experimental fuel.

3.1.2 *Hyperstoichiometric Fuel*

When the fuel rod becomes defective, an increase in the oxygen-to-uranium (O/U) ratio results in the direct enhancement of the diffusional release of fission products from the fuel matrix.[19,24,25, 26,27] Experimental work has indicated that xenon diffusion occurs as a neutral tri-vacancy in uranium dioxide,[27] in agreement with the theoretical calculations of Grimes and Catlow.[28] These calculations also indicate that in hyperstoichiometric fuel (UO_{2+x}), the most stable solution site is the uranium vacancy.[28] This finding supports the model of Killeen and Turnbull for the noble gas diffusion coefficient in UO_{2+x}.[19] In this model, it has been assumed that the gas atom mobility is influenced by the presence of the uranium cation vacancies in which Frenkel and Schottky equilibria govern the isolated point defects. Since the anion Frenkel defects predominate in urania, an increase in the oxygen interstitial concentration results in a reduction of the oxygen vacancy concentration; however, due to the secondary Schottky equilibrium, an increased uranium vacancy concentration results. This model for the diffusion coefficient is in agreement with annealing test results over the temperature range of 1000 to 1350°C in CO/CO_2, and with the experimental work of Lindner and Matzke.[19,24] The Killeen and Turnbull model is expected to be valid for small stoichiometry deviations (i.e., 0.005 to 0.1) but has been successful up to higher values of x of ~0.2.[19]

For the in-pile diffusion coefficient for hyperstoichiometric fuel, it is the vacancy-enhanced term in Eq. (16) that was modified to account for deviations from stoichiometry x.[19] Specifically, when uranium dioxide oxidizes to the non-stoichiometric UO_{2+x}, the extra oxygen is incorporated within the existing lattice as x interstitials per mole along with the $2x$ electron holes. On the existing sub-lattices there is a reduction in the number of oxygen vacancies and an increase in the number of uranium vacancies. Thus, the uranium vacancy concentration V_u is a function of x, where from the analysis of Lidiard:[29]

$$V_u = \frac{Sx^2}{F_o^2}\left[\frac{1}{2} + \frac{F_o}{x^2} + \frac{1}{2}\sqrt{1 + \frac{4F_o}{x^2}}\right]. \tag{20}$$

Here $F_o = \exp\{-Q_f/(RT)\}$ and $S = \exp\{-Q_s/(RT)\}$, where Q_f is the Frenkel energy for the oxygen lattice (71300 cal/mol) and Q_s is the Schottky energy (147200 cal/mol). The values of Q_f and Q_s were taken from the recommendations of Griesmeyer and Ghoniem.[30] In the model of Killeen and Turnbull, the uranium vacancy concentration V_u was substituted for V_o in Eq. (14):

$$V = \frac{\left(\alpha_s s^2 + Z_s V_u\right)}{2Z_s}\left\{\sqrt{1 + \frac{4KZ_s}{j_v\left(\alpha_s s^2 + Z_s V_u\right)^2}} - 1\right\}. \tag{21}$$

Equation (16) was then modified to account for both irradiation-enhanced and non-stoichometry effects by assuming a combined component of the form:

$$D_2(x,T) = s^2 j_v \left(V + V_u\right). \tag{22}$$

Combining all three components of Eqs. (13), (18) and (22) gives the effective in-pile diffusion coefficient proposed by Killeen and Turnbull for hyperstoichiometric fuel.[19] For experiments that are performed out-of-pile, $\dot{F}$ and V (i.e., $K = 0$ in Eq. (21)) have been set to zero due to the absence of fission fragment production.[31] In this case, the effective diffusion coefficient relevant to out-of-pile conditions becomes:

$$D = D_1(T) + D_2(x,T) = 7.6\times10^{-10}\exp\left\{\frac{-70000}{RT}\right\} + 4s^2 j_v V_u . \tag{23}$$

An extra factor of 4 has been similarly considered for the oxidation-enhanced component based on the analysis in Ref. 18. With oxidized fuel, one generally finds that $D_2(x,T) >> D_1(T)$.

It has been further recognized that for most values of x and T under consideration, the condition, $x^2 >> 4F_o$, will hold. For example, this requirement implies that at $T = 1000$ K, $x^2 >> 1 \times 10^{-15}$, whereas at a higher temperature of $T = 2000$ K, $x^2 >> 6 \times 10^{-8}$, i.e., these small values of x will yield an insignificant contribution of the vacancy-enhanced term to the overall diffusion coefficient. Thus, with this condition, V_u in Eq. (20) reduces to[31]

$$V_u \approx \frac{Sx^2}{F_o^2}, \quad \text{for } x^2 >> 4F_o . \tag{24}$$

Consequently, $D_2(x,T)$ in Eq. (23) can be written in the much simpler form

$$D_2(x,T) = x^2 D_{ox} \exp\left\{\frac{-Q_{ox}}{RT}\right\}, \quad \text{for } x^2 >> 4F_o \tag{25}$$

where D_{ox} and Q_{ox} are constants. For the analysis of Killeen and Turnbull, using the relation for $D_2(x,T)$ in Eq. (23) with V_u in Eq. (24), the constants in Eq. (25) are evaluated as $D_{ox} = 4.00 \times 10^{-6}$ m^2 s^{-1} and $Q_{ox} = 59800$ cal mol^{-1}. These constants have also been obtained for CANDU-type fuel with a fitting of the kinetic release data for cesium observed in several CRL annealing experiments in steam for stoichiometry deviations up to about 0.2. In this analysis, a combined (out-of-pile) effective diffusion coefficient consisting of Eq. (13) (for the intrinsic component) and Eq. (25) (for the non-stoichiometry enhanced vacancy component) was used. A fitting of the diffusion coefficient to release data from six HCE2 tests with both bare fuel fragments (i.e., CF2, CF3 and CF1) and mini-elements (i.e., CM2, CM6 and CM1), over the temperature range of 1350 to 1650 °C, yielded the following model parameters: $D_{ox} = 2.22 \times 10^{-8}$ m^2 s^{-1} and $Q_{ox} = 40200$ cal mol^{-1}.[31, 32] As shown in Fig. 8, the two sets of constants in Eq. (25) produce comparable results at higher temperature. In fact, the latter model of the diffusion coefficient (based on the CRL data fitting) has been successfully applied for the interpretation of high-temperature annealing experiments at various international laboratories.[31, 33]

Thus, for operating defective fuel rods, the solid-state diffusion coefficient for volatile fission products in UO_{2+x}, encompassing all aspects of intrinsic, athermal and vacancy-enhanced (from radiation and fuel oxidation) effects, can be given for the combined quantities in Eqs. (19) and (25) such that:

$$D(T,\dot{F},x) = 7.6\times10^{-10}\exp\left\{-\frac{70000}{RT}\right\} + 4\left[\sqrt{2}\times10^{-25}\sqrt{\dot{F}}\exp\left\{-\frac{27600}{RT}\right\} + 2\times10^{-40}\dot{F}\right] + x^2\,2.22\times10^{-8}\exp\left\{-\frac{40200}{RT}\right\}. \tag{26}$$

In order to employ Eq. (26), knowledge of the fuel oxidation kinetics (i.e., x as a function of time) is required for high pressure conditions which occur during normal defect operation (see Section 3.2).

3.2 *Fuel Oxidation Behaviour*

The UO_2 oxidation rate in steam-hydrogen mixtures at high temperature has been extensively studied in out-of-pile experiments, and the data interpreted by simple surface-exchange models in which the kinetics are constrained by equilibrium thermodynamics.[9] Unfortunately, all of these experiments are confined to atmospheric or sub-atmospheric pressures, and may not be pertinent to normal defect operation where the pressures are typically two orders of magnitude greater (i.e., approximately 100 atm). In addition, with operating fuel, there is a radiation field present which may further affect the fuel oxidation behaviour.

With the lack of such data, theoretical models based on mechanistic theory can be used to assess these effects. The high-pressure oxidation of the fuel by steam using adsorption theory is considered in Section 3.2.1. Radiolysis-assisted oxidation, through the possible production of strongly oxidizing and highly reactive products (e.g., H_2O_2 and perhaps O_2), in the presence of excess hydrogen, can also occur as a consequence of fission fragment bombardment of steam in the fuel-to-clad gap. This mechanism is also treated in Section 3.2.2 based on the limited experimental observations.

3.2.1 *High-Pressure Steam Oxidation*

The fuel oxidation process has been extensively studied at atmospheric pressure where it has been shown that the kinetics are controlled by a reaction at the solid/gas interface and not by the solid-state diffusion of oxygen. In this case, the fuel oxidation kinetics are described by the phenomenological model:[31]

$$c_U \left(\frac{V}{S}\right)_{fuel} \frac{dx}{dt} = c_U \alpha \{x_e - x(t)\} \tag{27}$$

where c_U is the molar density of uranium (= 4.0×10^4 mol of uranium m^{-3}), α is a surface exchange coefficient (= 0.365 exp{-23500/T(K)} m s^{-1}), x_e is the equilibrium stoichiometry deviation, and $(V/S)_{fuel}$ is the volume-to-surface area ratio of the fuel (m).The value of x_e in Eq. (27) is obtained by equating the oxygen potential (i.e., oxygen partial pressure) in the fuel (Appendix A.1) to that in the atmosphere (Appendix A.2).

As previously mentioned, the model in Eq. (27) is only specifically valid at atmospheric pressure (since α is fitted to the fuel oxidation experiments at this pressure). Therefore, this model cannot necessarily be extrapolated to the high-pressure situation which exists during normal defect operation. In this case, one must appeal to a more mechanistic treatment for extrapolation, such as the Langmuir adsorption theory:[9,10,36]

$$c_U \left(\frac{V}{S}\right)_{fuel} \frac{dx}{dt} = n_s k_a' \frac{A(T) P_{H_2O}}{1 + A(T) P_{H_2O}} \left[1 - \frac{q(x)}{P_{H_2O} / P_{H_2}} \right] \tag{28}$$

Here $n_s = 1.66 \times 10^{-6}$ mol m^{-2} is the density of adsorption sites which assumes a monolayer coverage of 10^{18} molecules m^{-2}. In Eq. (28), the oxygen activity $q(x)$ for a gas-solid equilibrium is defined as:

$$q(x) = \frac{\sqrt{P_{O_2}(x)}}{K_{H_2O}}. \tag{29}$$

For the H_2O decomposition reaction

$$H_2O \overset{K_{H_2O}}{\Leftrightarrow} H_2 + \tfrac{1}{2} O_2 \tag{30}$$

the equilibrium constant in Eq. (29) is evaluated at temperature T(K) from

$$K_{H_2O} = \frac{P_{H_2} \sqrt{P_{O_2}}}{P_{H_2O}} = \exp\left\{ 0.9794 \ln T - 1.1125 - \frac{28820}{T} \right\}. \tag{31}$$

In Eq. (28), P_{H_2O} and P_{H_2} are the partial pressures (in atm) of steam and hydrogen in the gap atmosphere after dissociation. In fact, using Eqs. (29) and (31), the quantity $q(x)/(P_{H_2O}/P_{H_2})$ in Eq. (28) simply equals $\sqrt{P_{O_2}(x)/P_{O_2}}$ where $P_{O_2}(x)$ pertains to the oxygen partial pressure in the fuel (Appendix A.1), and P_{O_2} refers to the oxygen partial pressure in the gap atmosphere (Appendix A.2). The parameter $A(T)$ (atm^{-1}) is defined as

$$A(T) = 1.0135 \times 10^5 \frac{s}{n_s k_a \sqrt{2 \pi R T M_{H_2O}}} \tag{32}$$

where T is the temperature (in K), R = 8.314 J mol^{-1} K^{-1} and $M_{H_2O} = 18 \times 10^{-3}$ kg mol^{-1}.

The desorption rate constant, k_a, the steam dissociation rate constant, k_a', and the sticking probability s in the model are obtained with a fitting of Eq. (28) to the predictions of Eq. (27) (at one atmsophere). It is acceptable to use the phenomenological model of Cox et al. in Eq. (27) as a representation of the fuel oxidation experience since it has been validated against numerous CRL experiments that were conducted in steam at atmospheric pressure.[31] The resultant kinetics for the models are shown in Fig. 9, using a Runge-Kutta method to solve for $x(t)$

in Eqs. (27) and (28). For the current analysis, the Blackburn model of Appendix A.1 was used to evaluate the oxygen partial pressure in the fuel. An $(S/V)_{\mathrm{fuel}}$ ratio of 329 m^{-1}, typical of a CANDU fuel rod, was also assumed in the calculation. The parameters resulting from this fitting are: $k_a = 10^{13} \exp\{-21557/T\}\ \mathrm{s}^{-1}$, $k_a' = 2.48\times10^{10} \exp\{-28105/T\}\ \mathrm{s}^{-1}$ and $s = 0.023$. This result is comparable with other fittings of Eq. (28) to the available fuel oxidation data.[9,10,36] The fitted value of the desorption rate constant is also consistent for that of a surface-bound species. For instance, the fitted value of the activation energy for k_a (i.e., ~43 kcal mol^{-1}) is typical of that expected for a chemisorption process for H_2O;[37] i.e., this type of process is expected in light of the requirement for a strong adsorbate-substrate bond at high temperature. The pre-exponential factor of $10^{13}\ \mathrm{s}^{-1}$ for k_a is also a physically-accepted value for the vibration frequency of an adsorbed molecule. In addition, the assumption of a single monolayer coverage for n_s is reasonable considering that a monolayer is not normally exceeded with chemisorption.

Without existing data for high-pressure fuel oxidation, one cannot rule out the possibility of a Freundlich isotherm in the adsorption model for the oxidation kinetics.[10] In particular, the surface coverage term for Langmuir adsorption in Eq. (28), i.e.,

$$\theta = \frac{A(T)P_{H_2O}}{1 + A(T)P_{H_2O}} \tag{33}$$

can be replaced by the corresponding Freundlich isotherm[37]

$$\theta = c_1 {P_{H_2O}}^{1/c_2} \tag{34}$$

in which $c_2 = 2$ in the present situation. Thus, a similar fitting yields:

$$c_U \left(\frac{V}{S}\right)_{fuel} \frac{dx}{dt} = n_s k_a' \sqrt{P_{H_2O}} \left[1 - \frac{q(x)}{P_{H_2O} / P_{H_2}}\right] \tag{35}$$

where , $k_a' = 1.04\times10^{9} \exp\{-23690/T\}\ \mathrm{s}^{-1}$. As expected, the latter activation energy for k_a' (i.e., 23,690 K) is similar to that for the surface-exchange coefficient α in Eq. (27) (i.e., 23,500 K). As shown in Fig. 10, both of the adsorption models are in good agreement with the phenomenological model of Eq. (27) (which is relevant to atmospheric pressure conditions). Moreover, both of the adsorption models are also able to reproduce the observed oxidation kinetics over the lower pressure range of 0.01 to 1 atm, where a roughly square-root dependence on the pressure is observed.[9,31,36] For instance, a square-root dependence on the steam pressure is directly observed in Eq. (35) for the Freundlich isotherm. The pressure dependence for the Langmuir model also arises from the surface coverage term in Eq. (33). Thus, in the H_2O/Ar experiments of Albrefah et al. (for steam pressures of 0.25 to 1 atm at 1623 K),[38] Eq. (32) yields a value of $A = 2.11\ \mathrm{atm}^{-1}$, and Eq. (33) subsequently predicts a reduction factor for the lower-pressure oxidation kinetics of: $2.11(1)/[2.11(1)+1] \div 2.11(0.25)/[2.11(0.25)+1] = 2.0$. This value is in excellent agreement with an observed square-root dependence of $(1/0.25)^{1/2} = 2.0$. Similarily, for the CEA He/H_2O experiments (i.e., for steam pressures of 0.01 to 0.03 atm at 1473 K),[31] with $A = 8.56$, a ratio of $8.56(.03)/[8.56(.03)+1] \div 8.56(.01)/[8.56(.01)+1] = 2.59$ is obtained. This value is also in good agreement with an observed ratio of $18.2/8.2 = 2.22$ in Fig. 6 of Ref. 31.

Thus, at atmospheric pressure, all of the models are in relative agreement since they are obtained from a fitting to the available fuel oxidation data at this pressure (see Figs. 9 and 10). In addition, the two adsorption models are able to explain the low pressure kinetics. However, on extrapolation to high pressure, i.e., relevant to defective fuel operation (e.g., 100 atm), a significant deviation occurs. For instance, at 1500 K in pure steam, $A = 6.5$ so that $\theta \sim 1$ for a steam pressure of 1 and 100 atm, and hence there is little effect of pressure in Eq. (33). Therefore, as shown in Fig. 11, both the phenomenological model and the Langmuir model are comparable (i.e., only the equilibrium value of the stoichiometry deviation is slightly affected in these models). On the other hand, there is a direct $\sqrt{P_{H_2O}}$ dependence for the Freundlich isotherm in Eq. (35), resulting in enhanced kinetics by an order of magnitude (i.e., $\sqrt{100}$) (see Fig. 11). Experiments are clearly required to confirm the high-pressure kinetics.

3.2.2 *Radiolysis-Assisted Fuel Oxidation*

Since the dose rate due to energy deposition from fission fragments in the steam-filled gap is two orders of magnitude higher than that from fast neutrons or gamma rays, the fission fragments can be considered as the major contributor of steam radiolysis in the gap of defective rods.[12] Although many free-radical intermediates are produced, the overall radiolytic reactions are:[13]

$$2H_2O \rightarrow H_2O_2 + H_2 \tag{36a}$$

$$2H_2O \rightarrow O_2 + 2H_2. \tag{36b}$$

The radiolysis products of steam (e.g., H_2O_2 and perhaps O_2) can oxidize the fuel. In particular, the formation of hydrogen peroxide, oxygen and hydrogen greatly exceeds their radically-induced recombination rate because of the strong fission fragment radiation field, and therefore the reactions in Eq. (36) do not reach thermodynamic equilibrium.[11,39,40,41] The highly-reactive hydrogen peroxide molecule, however, can equilibriate with the fuel and oxidize it even in the presence of a large excess of hydrogen.[13,39,40,41] Although a significant portion of the hydrogen that is liberated in the reactions of Eq. (36) may result in clad hydriding, it is not clear, however, if this other major radiolysis product could neutralize the tendency of its oxidizing counterparts to increase the stoichiometry of the fuel. Furthermore, as the temperature is raised, radiolytic effects should become insignificant to thermal effects as the thermal reactions and the recombination of transient species become faster.[12] Eventually, at a sufficiently high temperature, the thermal reactions will control the process of fuel oxidation.

Within the current level of uncertainty for the complex radiation chemistry of water vapour, the radiolysis effect can be modelled as a production of equal amounts of H_2O_2 and H_2 in accordance with Eq. (36a).[13] Since experiments show that H_2O_2 rapidly oxidizes UO_2 even in excess H_2,[42] it can be conservatively assumed that all of the H_2O_2 produced by steam radiolysis is consumed by the fuel-oxidation reaction.[13]

3.2.2.1 *Radiolysis Production Rate*

The volumetric rate of production Q^{rad} (mol m^{-3} s^{-1}) of the radiolytic products is derived as follows. In the fission process, ^{88}Br and ^{135}I can be considered as typical fragments, which obtain 101.5 and 66.5 MeV of the available fission energy at their point of birth in the fuel.[15] As they traverse through the fuel, their energy is lost by electronic and nuclear processes. The average energy of these fragments leaving the UO_2 fuel (of density 10.7 g cm^{-3}) can be determined from their energy-range relationships (see Fig. 12(a)) using the SRIM 2000 (Stopping and Range of Ions in Matter) code, which is based on a Monte Carlo treatment.[43] As shown in Fig. 12(a), the energy loss, dE/dx, can be reasonably approximated as a linear function of distance x:

$$\frac{dE}{dx} \approx -\left(\frac{2E_o}{r}\right)\left[1-\frac{x}{r}\right] \tag{37a}$$

$$\Rightarrow E(x) = E_o\left[1-\frac{x}{r}\right]^2, \tag{37b}$$

where r is the fission fragment range and E_o is the initial fission fragment energy (i.e., 101.5 for bromine and 66.5 MeV for iodine). Equation (37b) follows on integration of Eq. (37a) with the condition, $E(x=0) = E_o$. As shown in Fig. 12(a), a more accurate representation is obtained if the average range plus its straggling is used in Eq. (37a) (i.e., $r_{Br\text{-}88} = 8.70 + 0.68\ \mu\text{m} = 9.38\ \mu\text{m}$ and $r_{I\text{-}135} = 6.43 + 0.76\ \mu\text{m} = 7.19\ \mu\text{m}$) instead of just the average range itself.[43] The same relationship in Eq. (37b) has been proposed in Ref. 12. Thus, the average energy $<E>$ of the fission fragments leaving the UO_2 is simply obtained on use of Eq. (37b) where by definition:

$$< E >= \int_0^r E(x)dx \Big/ \int_0^r dx = \frac{E_o}{3}. \tag{38}$$

Therefore, a fragment with an initial energy E_o will be reduced by a factor of 3 (on average) as it enters into the fuel-to-clad gap. The high-energy fission fragments subsequently traverse through the thin annular gap of thickness h ~12.5 μm with a mean chord length $\bar{z} = 2\,h = 25$ μm.[15] As shown in Fig. 12(b), with the gap filled with steam at a density of 0.035 g cm^{-3}, only a small amount of energy loss occurs as the fragments eventually embed themselves in the adjacent clad wall.

Hence, the rate of production Q_j^{rad} (mol m^{-3} s^{-1}) due to steam radiolysis of molecule *j* (i.e., hydrogen or hydrogen peroxide) per unit volume in the gap is given by:

$$Q_j^{rad} = \frac{q_{H_2O} G_j \bar{z}}{N_{Av} V_{gap}} \sum_{i=I,Br} \left[\frac{1}{4} r_i S \dot{F} \right] LET_i . \tag{39}$$

The quantity in square brackets is the familiar recoil release rate of fission fragments from a solid fuel body.[11] Here N_{Av} is Avogadro's number (= 6.022 × 10^{23} molecule mol^{-1}), $\bar{z}$ is the path length in the gap (m), r_i is the fission fragment range in the fuel (= 9.38 × 10^{4} Å for ^{88}Br and 7.19 × 10^{4} Å for ^{135}I), *S* is the surface area of the fuel (m^2), V_{gap} is the gap volume (m^3), $\dot{F}$ is the fission rate density (fission m^{-3} s^{-1}) and *LET* is the fission fragment linear energy transfer (eV/Å). As a conservative calculation for the radiolysis analysis, the energy loss by bremsstrahlung radiation can be neglected so that the energy absorbed in the steam is equal to the energy loss in the gap.[44] Therfore, in Eq. (39), $LET = (dE/dx)_{loss}$, where the average energy loss in the gap over the given path length $\bar{z}$ is evaluated from Fig. 12(b) as $(dE/dx)_{loss}^{Br-88} \approx$ 15.7 eV/Å and $(dE/dx)_{loss}^{I-135} \approx$ 12.8 eV/Å. The parameter G_j is the G-value for the radiation yield of molecule *j* produced per 100 eV of ionizing energy deposited by the fission fragments in the water vapour molecules of the gas mixture. Here, the gas mixture in the gap has a steam mole fraction q_{H_2O}. Boyd and Miller studied fission fragment radiolysis of water vapour with and without various additives as a function of temperature (170 - 365°C) and density (1 – 50 mg mL^{-1}).[45] Based on this work, McCracken suggested a *G*-value ≈ 6.5/100 eV for oxidizing or reducing equivalents in water vapour in order to reflect the probable occurrence of impurity (uranium) species in the gap and possible reactions with the inner clad surface.[12] This value is also supported by the recent experimental work of Olander et al., where *G* ~ 8.5/100 eV for the H$_2$ radiolysis product with α-particle radiation in pure saturated steam at 70 atm.[1,42] Thus, in the present analysis, in accordance with Eq. (36a), it can be assumed that $G_{H_2} = G_{H_2O_2} = G \approx 6.5/100\,\text{eV}$.

Since the experiments show that H$_2$O$_2$ rapidly oxidizes the UO$_2$, even in the presence of excess H$_2$ (see Section 3.2.2), it can be assumed that all of the H$_2$O$_2$ produced by radiolysis is consumed in the fuel oxidation process. Thus, by neglecting gas phase recombination reactions involving H$_2$O$_2$ and the loss of this species by cladding corrosion, this assumption will yield an upper limit of the radiolytically-driven fuel oxidation rate. Hence, the rate at which the H$_2$O$_2$ is consumed per unit surface area of fuel is given by $R_{H_2O_2}^{ox}$ (in mol m^{-2} s^{-1}):

$$R_{H_2O_2}^{ox} = h Q^{rad} = \frac{q_{H_2O} G \bar{z} \dot{F}}{4 N_{Av}} \sum_{i=I,Br} \left[r \left(\frac{dE}{dx} \right)_{loss} \right]_i . \tag{40}$$

3.2.2.2 *Fuel Oxidation Kinetics*

The rate at which the fuel oxidizes is governed by the difference between the rates of oxidation by steam and hydrogen peroxide, and reduction by hydrogen. The thermodynamic model of Eqs. (27), (28) or (35) (see Section 3.2.1) accounts for the fuel oxidation and reduction reaction rates in the presence of a gaseous mixture of hydrogen and steam. This process is limited by a thermodynamic constraint that stops the reaction when the equilibrium stoichiometry deviation is reached (see Figs. 9 to 11). In contrast, the (maximum) radiolytically-driven fuel oxidation rate in Eq. (40) (see Section 3.2.2) is not thermodynamically limited. Hence, the conservation equation for the oxygen balance in the fuel is:[13,42]

$$c_U \left(\frac{V}{S} \right)_{fuel} \frac{dx}{dt} = R_{H_2O_2}^{ox} + R_{H_2O}^{ox} - R_{H_2}^{red} , \tag{41}$$

where

$$R_{H_2O}^{ox} - R_{H_2}^{red} = f(T, P_{H_2O})\left\{1 - \sqrt{P_{O_2}(x)/P_{O_2}}\right\}. \tag{42}$$

Here the function $f(T, P_{H_2O})$ depends on the choice of the adsorption isotherm (see Section 3.2.1)

$$f(T, P_{H_2O}) = \left\{\begin{matrix} n_s k_a' \dfrac{A(T)P_{H_2O}}{1 + A(T)P_{H_2O}} & (Langmuir) \\ n_s k_a' \sqrt{P_{H_2O}} & (Freundlich) \end{matrix}\right\}. \tag{43}$$

Alternatively, at atmospheric pressure, Eq. (27) can also be used for $R_{H_2O}^{ox} - R_{H_2}^{red}$. For the oxygen balance of Eq. (41), it has been implicitly assumed that the rate of fuel oxidation by hydrogen peroxide results from the reaction:[42]

$$H_2O_2(g) \rightarrow O(s) + H_2O(g), \tag{44}$$

where *O*(*s*) represents oxygen in the fuel above the normal O/U ratio of two. The P_{O_2} in Eq. (42) is evaluated in Appendix A.2, based on the initial quantities of H_2O and H_2 in the gap atmosphere prior to dissociation.

Equation (41) can be used to assess the fuel oxidation kinetics in the CRL experiment, FFO-103, where a CANDU-size fuel rod was machined with 23 slits along the entire length of the cladding.[11] This experiment was designed to minimize the holdup of fission products in the fuel-to-clad gap, and to permit unrestricted coolant entry so as to maximize the fuel oxidation. The defected fuel rod operated in-reactor at a linear power of 50 kW/m (i.e., a fission density rate of 1.35×10^{19} fission m^{-3} s^{-1}) in a pressurized water loop at 100 atm. Based on an analysis with the ELESIM fuel performance code, the experimental rod had an average fuel temperature of 1550 K.[46] In this analysis, it can be assumed that the gap is essentially filled with pure steam, implying an oxygen partial pressure of 3.23×10^{-3} atm (Appendix A.2). The solution of the fuel oxidation model in Eqs. (40), (41) and (42) (with the Langmuir adsorption isotherm) is shown in Fig. 13, with and without radiolysis-assisted fuel oxidation. When coolant radiolysis is taken into consideration, the kinetics are more rapid and a slightly higher equilibrium stoichiometry deviation results. An equilibrium stoichiometry deviation of 0.28 was measured by gravimetric analysis after 15 d of operation. This measured value was in fact higher than that predicted by equilibrium thermodynamics (using the Blackburn model in Appendix A.1) for steam oxidation in Fig. 13 (i.e., 0.24); however, it was in good agreement with the predicted value of 0.28 with radiolysis-assisted oxidation.[11] The oxidation/reduction in Eq. (42) actually limits the overall equilibrium stoichiometry deviation in Eq. (41). Here, the increased $P_{O_2}(x)$ is eventually higher than the value of the atmospheric P_{O_2} (for pure steam) in Eq. (42) so that a reduction actually occurs (i.e., $R_{H_2O}^{ox} - R_{H_2}^{red} < 0$). Thus, this resulting negative term is eventually balanced by the radiolysis term in Eq. (41) so that an equilibrium oxidation situation is established. This equilibrium is rapidly reached as shown in Fig. 13. This prediction is also supported from the observed fission product release behaviour, which showed a relatively constant release rate over the course of the experiment for those isotopes that had quickly reached radioactive equilibrium.[11]

For typical defective rods, where the coolant entry is more limited, hydrogen liberated in the oxidation reactions will reduce the oxygen potential in the gap and hence the amount of fuel oxidation. The steam must also diffuse into the gap as a source from the defect site. Thus, under normal defect occurrences, the P_{O_2} in Eq. (42) must be evaluated for the relevant hydrogen/steam mixture in the gap. The mass balance equations for hydrogen and steam transport in the gap are detailed in Section 3.2.2.3.

3.2.2.3 *Hydrogen and Steam Mass Balance in the Gap*

For a solution of Eq. (41), the partial pressures of hydrogen and steam must be known *a priori*. Hence, mass balance equations are also required for the determination of the concentration profiles of the gaseous constituents in the gap. At normal operating conditions, one can generally neglect the small amount of fission gas and hydrogen peroxide present in the atmospheric mixture. In this case, the mole fractions of hydrogen (q_{H_2}) and steam (q_{H_2O}) must sum to unity, i.e.,[42]

$$q_{H_2} = 1 - q_{H_2O}. \tag{45}$$

Hence, only a mass balance equation for steam is required.

The general conservation equation for the molar concentration c_i (= cq_i) of any component i (i.e., i = H_2 and H_2O) in the fuel-to-clad gap is:[10,47]

$$\frac{\partial c_i}{\partial t} = -\frac{\partial J_i}{\partial z} + Q_i - R_i. \tag{46}$$

Here q_i is the mole fraction of the given constituent in the gap, J_i is the molar flux of component i, Q_i and R_i are the production and loss rates, respectively, and c is the total molar concentration (mol m^{-3} s^{-1}) as determined from the ideal gas law:

$$c = \frac{P_{tot}}{RT}. \tag{47}$$

The molar flux of component i results from both diffusion and a total molar bulk flow J:[10,47]

$$J_i = -cD\frac{\partial q_i}{\partial z} + q_i J \tag{48}$$

The diffusivity parameter cD (mol m^{-1} s^{-1}) can be evaluated from Chapman-Enskog kinetic theory for a binary mixture (i.e., hydrogen and steam) (see Appendix A of Ref. 10). Thus, using Eq. (48), and assuming that during normal operation the total pressure in the gap is time-independent with no pressure gradients (so that from Eq. (47) the total molar concentration is constant), Eq. (46) becomes

$$c\frac{\partial q_i}{\partial t} = cD\frac{\partial^2 q_i}{\partial z^2} - \frac{\partial (q_i J)}{\partial z} + Q_i - R_i. \tag{49}$$

Neglecting any production of steam in the gap from the homogeneous recombination of H_2 and H_2O_2, the source term Q_i will therefore be equal to zero. Steam losses in the gap will result from radiolysis (R^{rad}), and oxidation of the fuel (R_f^{ox}) and cladding (R_c^{ox}). Thus, for the steam species (i = H_2O), Eq. (49) can be written as

$$c\frac{\partial q_{H_2O}}{\partial t} = cD\frac{\partial^2 q_{H_2O}}{\partial z^2} - \frac{\partial (q_{H_2O} J)}{\partial z} - R^{rad} - R_f^{ox} - R_c^{ox}. \tag{50}$$

The steam loss rate due to radiolysis R^{rad} (mol m^{-3} s^{-1}) is determined from Eq. (40), i.e.,

$$R^{rad} = \frac{R_{H_2O_2}^{ox}}{h}. \tag{51}$$

Similarly, the loss rate from fuel oxidation R_f^{ox} (mol m^{-3} s^{-1}) is derived from Eq. (42):

$$R^{rad} = \frac{R_{H_2O_2}^{ox} - R_{H_2}^{red}}{h}. \tag{52}$$

The loss rate from Zircaloy oxidation R_c^{ox} (mol m^{-3} s^{-1}) follows from Ref. 11:

$$R_c^{ox} = \frac{7.85\times 10^3 \exp\{-14190/T\}}{h} \tag{53}$$

where h is the gap thickness (m) and T is the inside clad temperature (K). Equation (53) is based on a weight gain which is linear with time, and is consistent with the linear rate kinetics observed at 350°C for the oxidation of sponge zirconium in the experiments of Ref. 42.

For the total gas balance in the gap, the conservation statement of Eq. (46) yields:

$$\frac{\partial c}{\partial t} = -\frac{\partial J}{\partial z} - \frac{R_H^{hyd}}{2h}, \tag{54}$$

where the only loss of gas results from hydrogen removal by the cladding due to hydrogen pickup and massive hydriding R_H^{hyd} (mol m^{-2} s^{-1}). The quantity R_H^{hyd} is derived, for example, from the experiments that are detailed in Ref. 42. The factor of 2 arises from the definition of the rates of hydrogen absorption in terms of moles of H (rather than for gaseous H_2). Since the total pressure (and therefore c) is time–invariant at normal operating conditions, Eq. (54) yields

$$\frac{\partial J}{\partial z} = -\frac{R_H^{hyd}}{2h}. \tag{55}$$

Hence, in the case of a large defect (i.e., typical of the FFO-103 rod), where the H_2O/H_2 ratio is above a critical ratio, hydriding will not occur so that $R_H^{hyd} = 0$.[11] It therefore follows in this situation that the gradient of the molar gas flow in the gap is zero in Eqs. (55) (and in Eq. (50) as well).

For a solution of Eq. (50), one initial condition and two boundary conditions are required. For example, in the CRL experiment FFO-102-2, a secondary hydride failure occurred at the end of the rod, i.e., at $x = l$ in Fig. 1.[11] In this case, the initial and boundary conditions can be described by:

$$q_{H_2O} = 1, \quad \text{at } t = 0, 0 < x < l, \tag{56a}$$

$$\frac{\partial q_{H_2O}}{\partial z} = 0, \quad \text{at } x = 0, t > 0, \tag{56b}$$

$$q_{H_2O} = 1, \quad \text{at } x = l, t > 0. \tag{56c}$$

Equation (56a) implicitly assumes that steam is initially present in the gap. The boundary condition in Eq. (56b), indicates no flow at the intact end of the rod (i.e., a reflexive condition), while Eq. (56c) imposes a continuous source of steam at the defect end as a result of coolant entry.

The solution of this type of equation requires a general numerical approach as detailed in Ref. 48.

4. CORRELATION FOR DEFECTIVE FUEL ROD POWER

A methodology has been established in Section 3 to determine the fuel oxidation kinetics in operating defective rods at high pressure, and its impact on the fission product diffusivity. Thus, the correlation in Fig. 7 for intact fuel can be corrected to account for enhanced diffusivity effects in defective rods. This modified correlation provides the means to predict the defective rod power by sampling the (short-lived) coolant activity at different power levels.

Generally, the mass balance equation for steam in Eq. (50), and for hydrogen in Eq. (45), must be solved in order to estimate the oxygen partial pressure in the gap atmosphere. As an alternative approach, the fuel oxidation model can be used in a reverse fashion to determine the typical hydrogen-to-steam partial pressure ratio that must have existed in the gap to yield an observed fuel oxidation state in a given defective rod. As seen in Fig. 13, the equilibrium oxidation state is obtained quite rapidly (i.e., within a day or so of operation). Moreover, there is not a great difference in the predicted equilibrium value using models with only steam oxidation and with radiolysis-assisted oxidation. Consequently, the equilibrium model of Appendix A can be used to determine the partial pressure ratio of hydrogen-to-steam in this calculation. For such an analysis, the natural defect experiment, FFO-102-2, is typical of an in-reactor hydride failure. This rod had operated in a high pressure coolant of 100 atm with an estimated average fuel temperature of 1574 K.[11] A post-test gravimetric analysis yielded a value of $x_e \sim 0.14$. Thus, a value of $P_{H_2O} / P_{H_2} \sim 0.1\%$ is obtained with the equilibrium model of Appendix A to match the measured end-of-test equilibrium stoichiometry deviation in this experiment.

As shown in Fig. 14, this representative ratio can be used to predict the equilibrium stoichiometry deviation, x_e, as a function of the fuel rod power (and average fuel temperature).[46] Hence, an empirical diffusivity (D') can be determined for defective fuel by scaling the sweep gas data (for unoxidized fuel) in Fig. 7 by a correction factor H such that[46]

$$D'_{defect} = HD'_{sweep\ gas}, \tag{57}$$

where

$$H = \frac{D(x_e,T)}{D(0,T)}. \tag{58}$$

Here the diffusion coefficient D is evaluated for the calculated value of x_e and the average fuel temperature T based on the model in Eq. (26).

This methodology can be tested against the empirical diffusivity correlation for noble gas (D'_s) in Table 1, as derived from a number of in-reactor defect experiments at CRL.[11] For example, this comparison is shown for a low and high-powered rod in Table 2. In this calculation, the correction factor of 4, used to account for recoil effects in the diffusion components of D_2 (Eq. (17)) and D_3 (Eq. (18)), has not been applied. The same implementation of the model was used for the ELESIM defective fuel calculations in Ref. 46. The good agreement in Table 2 (i.e., typically within a factor of 2), suggests that the sweep gas data in Fig. 7 can be suitably scaled. As such, the ratio of the noble gas release rate $R \propto \sqrt{D'}$ (see Eq. (5)) for a defected rod operating at two power steps (e.g., 100 and 50% of full power (FP)) will yield a unique signature ratio as shown in Table 2. This method exploits the composite nature of the diffusion coefficient in Eq. (26).

Table 2: Empirical Diffusion Coefficient for Defective Fuel

<table>
<tr><td colspan="5">*Comparison with CRL Experiments*</td></tr>
<tr><td>Linear Power (kW/m)</td><td>$H = D(x_e,T)/D(0,T)$[(a)]</td><td>$D'_{sweep\ gas}$ (s^{-1})</td><td>D'_{defect} (s^{-1})</td><td>D'_s (s^{-1})[(b)]</td></tr>
<tr><td>30</td><td>139</td><td>7.1×10^{-14}</td><td>9.8×10^{-12}</td><td>2.2×10^{-11}</td></tr>
<tr><td>60</td><td>4630</td><td>4.4×10^{-12}</td><td>2.0×10^{-8}</td><td>8.7×10^{-9}</td></tr>
<tr><td colspan="5">*Empirical Diffusion Coefficient Ratio at Full and Half-Power ($D'_{100\%FP}/D'_{50\%FP}$)*</td></tr>
<tr><td>Linear Power (kW/m)</td><td colspan="2">Sweep Gas</td><td colspan="2">Defect Fuel</td></tr>
<tr><td>60/30</td><td colspan="2">62</td><td colspan="2">2100</td></tr>
<tr><td>40/20</td><td colspan="2">5.7</td><td colspan="2">600</td></tr>
<tr><td>20/10</td><td colspan="2">1.5</td><td colspan="2">12</td></tr>
</table>

(a) Does not include the correction factor of 4 in Eq. (26).
(b) Derived from the correlation in Table 1.

5. CONCLUSIONS

The fission product release models for defective fuel have been reviewed for the various analysis packages used for fuel-failure monitoring in LWR and CANDU reactors. These models generally assume a diffusive release of fission products from the fuel matrix, with a subsequent transport in the gap based on first-order rate theory. Since the low-temperature release of fission products from tramp uranium deposited on in-core surfaces is a due to a recoil process, these two sources of coolant activity can be easily distinguished. Thus, with previous experience, it is possible to determine the number of fuel failures, the average defect size and location, and the fuel burnup and power with a coolant activity analysis.

A model has been developed to describe the fuel oxidation kinetics in operating defective rods. This model accounts for high-pressure oxidation in steam/hydrogen mixtures, based on Langmuir and Freundlich adsorption theory, and also considers radiolysis-assisted oxidation as a result of hydrogen peroxide production. Both isotherms predict a square root dependence on pressure from 0.01 to 1 atm in agreement with experimental data. However, on extrapolation to high pressure (e.g., 100 atm), the predictions deviate where the Freundlich isotherm predicts faster kinetics. High-pressure experiments are still required to determine which kinetics are appropriate. Radiolysis-assisted oxidation also appears to accelerate the kinetics; however, this effect only results in a slightly higher equilbrium fuel oxidation state than that predicted by thermodynamic theory. Nevertheless, all models indicate that an equilibrium oxidation state will be approached in defective rods, as supported (indirectly) by observations of the fission product release in the in-reactor CRL experiments.

The fuel oxidation models indicate that the equilibrium oxidation state of the defective fuel rod is achieved within a day of reactor operation. Consequently, it is possible to use the equilibrium quantity to calculate the fission product diffusivity in defective fuel. Thus, a correlation is possible to predict the fuel rod power because of the composite nature for this diffusion coefficient, which depends on vacancy-enhanced effects due to radiation damage and non-stoichiometry, as well as effects due to intrinsic (i.e., temperature driven) and athermal phenomena. A correlation can therefore be developed, based on a measurement of the (steady-state) coolant activity at different reactor power levels.

APPENDIX A: OXYGEN PARTIAL PRESSURE IN THE FUEL AND GAP ATMOSPHERE

A.1 Oxygen Partial Pressure in the Fuel

The oxygen partial pressure in the fuel as a function of x, i.e., $P_{O_2}(x)$ (in atm), is given by either the Blackburn thermochemical model:[34]

$$\ln P_{O_2} = 2\ln\left(\frac{x(2+x)}{1-x}\right) + 108x^2 - \frac{32700}{T} + 9.92 \tag{A.1}$$

or the solid solution representation of Lindemer and Bessman:[35]

$$P_{O_2} = \min(P_1, P_2) \tag{A.2}$$

where P_1 and P_2 are given by:

$$\ln P_1 = 2\ln\left(\frac{x(1-2x)^2}{(1-3x)^3}\right) - \frac{37621}{T} + 15.15, \tag{A.3}$$

$$\ln P_2 = 4\ln\left(\frac{2x(1-2x)}{(1-4x)^2}\right) - \frac{43298}{T} + 25.74.$$

A.2 Oxygen Partial Pressure in the Gap

The oxygen potential in the gap atmosphere (consisting of H_2O and H_2) is determined as follows.[10] The total pressure P_{tot} (atm) in the gap is derived from the constituent partial pressures P_j:

$$P_{tot} = \sum_{j=1}^{n} P_j \tag{A.4}$$

The equilibrium constant K_{H_2O} for the H_2O decomposition reaction is given in Eq. (31). If the H_2O dissociation required to maintain equilibrium is β, the partial pressures after dissociation are

$$P_{H_2O} = P^o_{H_2O} - \beta, \quad P_{H_2} = P^o_{H_2} + \beta, \quad P_{O_2} = \frac{\beta}{2} \tag{A.5}$$

where the superscript "o" refers to the initial partial pressures in the gap. Hence, the conditions for equilibrium can be described by combining Eqs. (31), (A.4) and (A.5),

$$K_{H_2O} = \frac{P^o_{H_2} + \beta}{P^o_{H_2O} - \beta} \times \sqrt{\frac{P_{tot}\left(\frac{1}{2}\beta\right)}{P^o_{H_2O} + P^o_{H_2} + \frac{1}{2}\beta}}. \qquad \text{(A.6)}$$

Equation (A.6) can be solved for β on evaluating the equilibrium constant in Eq. (31) for the given temperature T and knowing the initial partial pressures. The resulting partial pressures are:

$$\frac{P_{H_2}}{P_{tot}} = \frac{P^o_{H_2} + \beta}{\sum_{j=1}^{n} P_j}, \quad \frac{P_{H_2O}}{P_{tot}} = \frac{P^o_{H_2O} - \beta}{\sum_{j=1}^{n} P_j}, \quad \frac{P_{O_2}}{P_{tot}} = \frac{\frac{1}{2}\beta}{\sum_{j=1}^{n} P_j}, \qquad \text{(A.7)}$$

where $\sum_{j=1}^{n} P_j = P^o_{H_2O} + P^o_{H_2} + \frac{1}{2}\beta$.

ACKNOWLEDGEMENTS

The present work was supported by the Natural Sciences and Engineering Research Council of Canada, the Academic Research Program of the Department of National Defence (DND) and the Director General of Nuclear Safety of DND.

REFERENCES

1. R. Beraha, G. Beuken, G. Frejaville, C. Leuthrot and Y. Musante, "Fuel Survey in the Light Water Reactors Based on the Activity of the Fission Products," Nucl. Technol. 49 (1980) 426.
2. C. Leuthrot, and A. Brissaud, "SADAME - An On Line Computer Code to Assess in Operation Defective Fuel Characteristics and Primary Circuit Contamination," Proc. Int. Top. Mtg. LWR Fuel Performance, West Palm Beach, Florida, April 17-21, 1994.
3. C. Leuthrot, J.B. Genin, P. Ridoux and A. Harrer, "SADDAM - An On Line Computer Code to Assess in Operation Defective Fuel Characteristics and Primary Circuit Contamination," Proc. Int. Top. Mtg. LWR Fuel Performance, Portland, Oregon, March 2-6, 1997.
4. C.E. Beyer, "Methodology for Estimating Number of Failed Fuel Rods and Defect Size," EPRI NP-6554, September 1989.
5. D.L. Burman, O.A. Correal, H.W. Wilson, H. Kunishi and L.H. Boman, "Development of a Coolant Activity Evaluation Model and Related Application Experience," Proc. Int. Top. Mtg. LWR Fuel Performance, Avignon, France, April 21-24, 1991.
6. D.W.C. Lin, "An Improved Model for Estimating the Number and Size of Defected Fuel Rods in an Operating Reactor," Proc. Int. Top. Mtg. LWR Fuel Performance, West Palm Beach, Florida, April 17-21, 1994.
7. B.J. Lewis, R.J. Green and C.W.T. Che, "A Prototype Expert System for the Monitoring of Defected Nuclear Fuel Elements in Canada Deuterium Uranium Reactors," Nucl. Technol. 98 (1992) 307.
8. R.J. White and J.A. Turnbull, "The Study of Defective Fuel Using Primary Coolant Analysis," Proc. Int. Top. Mtg. LWR Fuel Performance, West Palm Beach, Florida, April 17-21, 1994.
9. D.R. Olander, "Mechanistic Interpretations of UO_2 Oxidation," J. Nucl. Mater. 252(1998) 121.
10. B.J. Lewis, "Prediction of the Oxygen Potential in the Fuel-to-Clad Gap during Severe Reactor Accident Conditions," J. Nucl. Mater., in press.
11. B.J. Lewis, R.D. MacDonald, N.V. Ivanoff and F.C. Iglesias, "Fuel Performance and Fission Product Studies for Defected Fuel Elements, Nucl. Technol. 103 (1993) 220.
12. D.R. McCracken, "Radiolytic Effects in Fuel Degradation," AECL-11353, May 1995.
13. D.R. Olander, W.E. Wang, Y. Kim, C.Y. Li, S. Lim and S.K. Suresh, "Investigation of the Roles of Corrosion and Hydriding of Barrier Cladding and Fuel Pellet Oxidation in BWR Fuel Degradation," Proc. Int. Top. Mtg. LWR Fuel Performance, Portland, Oregon, March 2-6, 1997.

14. B.J. Lewis, "A Generalized Model for Fission-Product Transport in the Fuel-to-Sheath Gap of Defective Fuel Elements," J. Nucl. Mater. 175 (1990) 218.
15. B.J. Lewis, "Fission Product Release from Nuclear Fuel by Recoil and Knockout," J. Nucl. Mater. 148 (1987) 28.
16. I.J. Hastings, C.E.L. Hunt, J.J. Lipsett and R.D. Delaney," Short-Lived Fission Product Release from the Surface and Centre of Operating UO_2 Fuel," AECL-8353, Atomic Energy of Canada Limited (1984).
17. J.A. Turnbull, C.A. Friskney, J.R. Findlay, F.A. Johnson and A.J. Walter, "The Diffusion Coefficients of Gaseous and Volatile Species during the Irradiation of Uranium Dioxide," J. Nucl. Mater. 107 (1982) 168.
18. J.A. Turnbull, R.J. White and C. Wise, "The Diffusion Coefficient for Fission Gas Atoms in Uranium Dioxide," Proceedings of the International Atomic Energy Agency Technical Committee Meeting on Water Reactor Fuel Element Computer Modelling in Steady State, Transient and Accident Conditions, Preston, England, 18-22 September 1988.
19. J.C. Killeen and J.A. Turnbull, "An Experimental and Theoretical Treatment of the Release of Kr from Hyperstoichiometric Uranium Dioxide," Proc. Workshop Chemical Reactivity of Oxide Fuel and Fission Product Release, Gloucestershire, England, April 7-9, 1987, p. 387, Central Electricity Generating Board.
20. D. Davies and G. Long, Report No. 4347, Atomic Energy Research Establishment (1963).
21. J.V. Sharp, "Radiation Enhanced Diffusion," Report No. 6267, Atomic Energy Research Establishment (1969).
22. Hj. Matzke, Proc. Workshop on Fission Gas Behaviour in Nuclear Fuels, Karlsruhe, EUR 6600, October 26-27, 1978.
23. L.D. MacDonald, D.B. Duncan, B.J. Lewis, F.C. Iglesias, L.N. Carlucci and D.F. Simmons, "FREEDOM 1.2: A Transient Fission-Product Release Model for Radioactive and Stable Species," RC-462, Chalk River Laboratories, July 1990.
24. R. Lindner and H. Matzke, Z. Naturforschg 14a (1959) 582.
25. W. Miekeley and F. Felix, J. Nucl. Mater. 42 (1972) 297.
26. G.T. Lawrence, "A Review of the Diffusion Coefficient of Fission-Product Rare Gases in Uranium Dioxide," J. Nucl. Mater. 71 (1978) 195.
27. H. Matzke, "Gas Release Mechanisms in UO_2 – A Critical Review," Radiation Effects 53 (1980) 219.
28. R.W. Grimes and C.R. Catlow, "The Stability of Fission Products in Uranium Dioxide," Phil. Trans. R. Soc. Lond. A 335 (1991) 609.
29. A.B. Lidiard, "Self-Diffusion of Uranium in UO_2," J. Nucl. Mater. 19 (1966) 106.
30. J.M. Griesmeyer and N.M. Ghoniem, J. Nucl. Mater. 80 (1979) 88.
31. B.J. Lewis, B. Andre, B. Morel, P. Dehaudt, D. Maro, P.L. Purdy, D.S. Cox, F.C. Iglesias, M.F. Osborne and R.A. Lorenz, "Modelling the Release Behaviour of Cesium During Severe Fuel Degradation," J. Nucl. Mater. 227 (1995) 83.
32. P.L. Purdy, B.J. Lewis, W.S. Andrews, D.S. Cox and F.C. Iglesias, "A Model for Fuel Oxidation and Diffusion-Based Fission Product Release Under Severe Nuclear Reactor Accident Conditions," Proceedings of the 4th International Conference on CANDU Fuel, ISBN 0-919784-52-6, Pembroke, Ontario, October 1-4, 1995, p. 5B 57.
33. B.J. Lewis, B.J. Corse, W.T. Thompson, M.H. Kaye, F.C. Iglesias, P.Elder, R. Dickson and Z. Liu, "Low Volatile Fission-Product Release and Fuel Volatilization During Severe Reactor Accident Conditions," J. Nucl. Mater. 252 (1998) 235.
34. P.E. Blackburn, J. Nucl. Mater. 46 (1973) 244.
35. T.B. Lindemer and T.M. Besmann, J. Nucl. Mater. 130 (1985) 473.
36. B.V. Dobrov, V.V. Likhanskii, V.D. Orzin, A.A. Solodov, M.P. Kissane and H. Manenc, "Kinetics of UO_2 Oxidation in Steam Atmosphere," J. Nucl. Mater. 255 (1998) 59.
37. P. Atkins, "Physical Chemistry," 5th edition, W.H. Freeman and Company, New York, 1994.
38. J. Albrefah, A. de Aguiar Braid, W. Wang, Y. Khalil and D.R. Olander, "High Temperature Oxidation of UO_2 in Steam-Hydrogen Mixtures," J. Nucl. Mater. 298 (1994) 98.
39. J.M. Markowitz, "Internal Zirconium Hydride Formation in Zircaloy Fuel Element Cladding Under Irradiation," WAPD-TM-351, Bettis Atomic Power Laboratory (May 1963).
40. J.C. Clayton, "Internal Hydriding in Irradiated Defected Zircaloy Fuel Rods," Proc. 8th Int. Symp. Zirconium in the Nuclear Industry, STP 1023, p. 266, American Society for Testing and Materials (1989).
41. D.R. Olander and S. Vakin, "Secondary Hydriding of Defected Zircaloy-Clad Fuel Rods," EPRI TR-101773, 1993.

42. D.R. Olander, W. Wang, Y.S. Kim, C. Li and K. Lim, "Chemistry of Defective Light Water Reactor Fuel," EPRI TR-107074, February 1997.
43. J. F. Ziegler and J.P Biersack, "SRIM: The Stopping and Range of Ions in Matter, SRIM-2000 (v. 09), IBM-Research, Yorktown, New York, 1998.
44. G.R. Choppin and J. Rydberg, "Nuclear Chemistry Theory and Applications," Pergamon Press, Oxford, England, 1980, p. 311.
45. A.W. Boyd and O.A. Miller, "Radiolysis of Water Vapour with Fission Fragments," Can. J. Chem. vol. 46, p. 3773, 1968.
46. B.J. Lewis, F.C. Iglesias, D.S. Cox and E. Gheorghiu, "A Model for Fission Gas Release and Fuel Oxidation Behavior for Defected UO_2 Fuel Elements," Nucl. Technol. 92 (1990) 353.
47. R.B. Bird, W.E. Stewart and E.N. Lightfoot, "Transport Phenomena," Wiley, New York, 1960.
48. B.J. Lewis and D.S. Cole, "Oxygen Potential in the Gap of Defective CANDU Fuel Rods during Severe Accident Conditions," Proc. 6th International Conference on CANDU Fuel, Niagra-on-the-Lake, September 26-29, 1999.

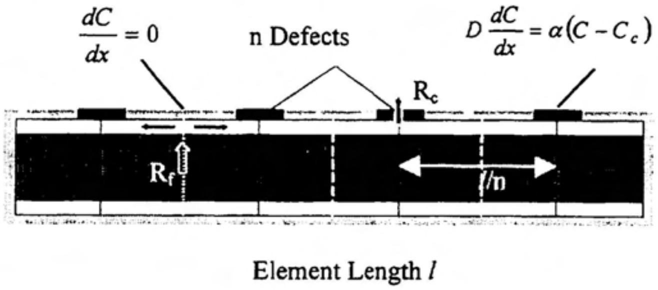

Figure 1. Schematic of defective fuel rod.

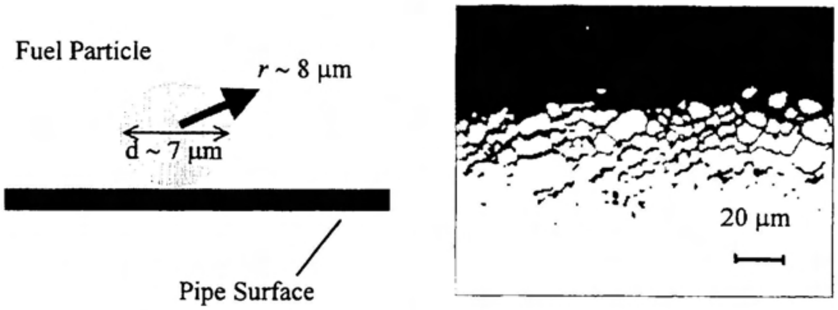

Figure 2. Tramp uranium fuel particle siting on a piping surface. The photograph shows the release of fuel, as a consequence of grain boundary oxidation, under a defect site.

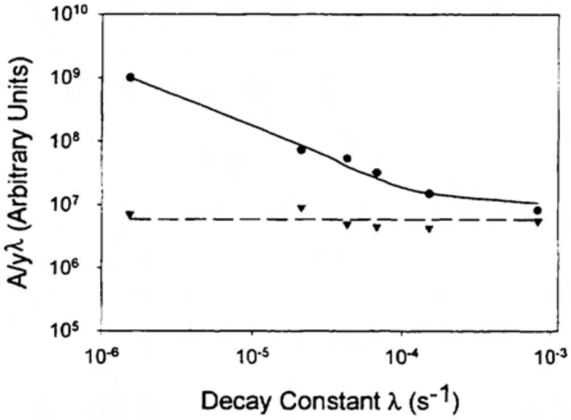

Figure 3. Off-gas coolant activity analysis for a BWR Plant showing the fission product from tramp uranium (i.e., prior to the occurrence of a defect) and after the occurrence of a fuel failure. The fitted lines employ the models in Eqs. (6) and (7).

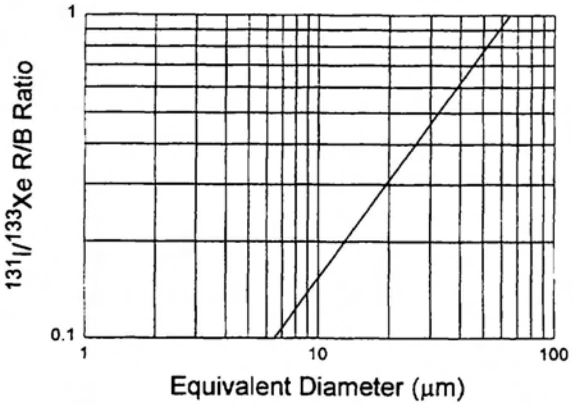

Figure 4. Correlation used in SADDAM to determine defect size from the R/B ratio of $^{131}I/^{133}Xe$.

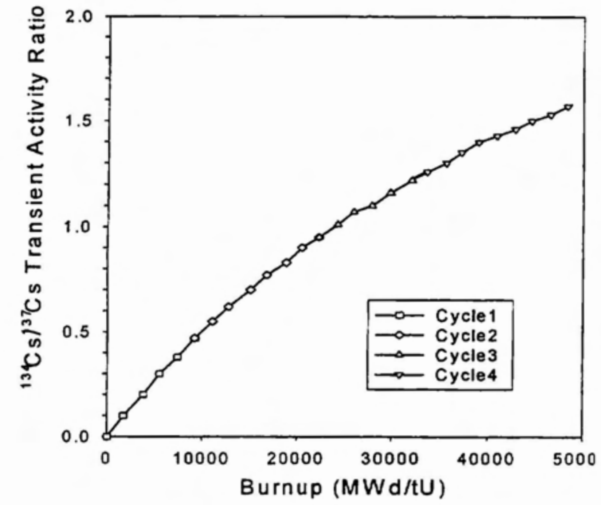

Figure 5. Correlation used in SADDAM to determine the burnup of defective fuel from the measured $^{134}Cs/^{137}Cs$ (transient) coolant activity ratio.

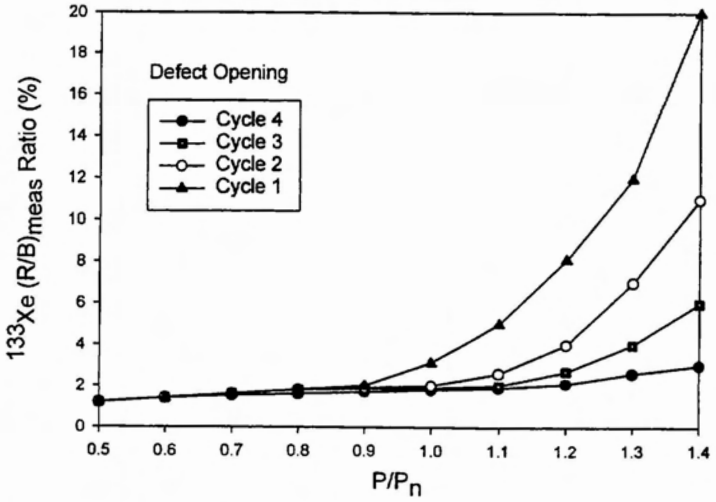

Figure 6. ^{133}Xe release-to-birth rate ratio versus rod linear power.

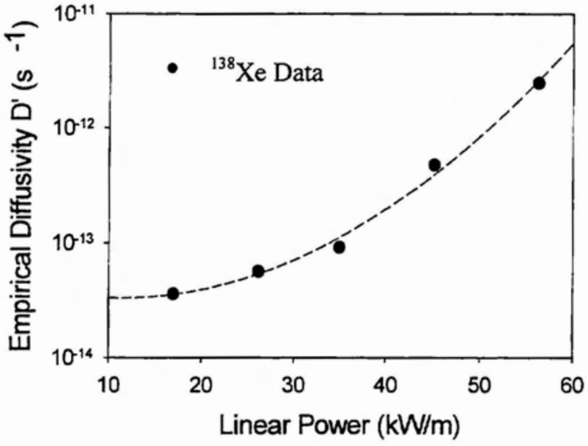

Figure 7. Empirical diffusion coefficients for ^{138}Xe versus linear power for intact rods for a step startup (CRL sweep gas experiment FIO-141). The reactor power was held for 1 h at each power level.

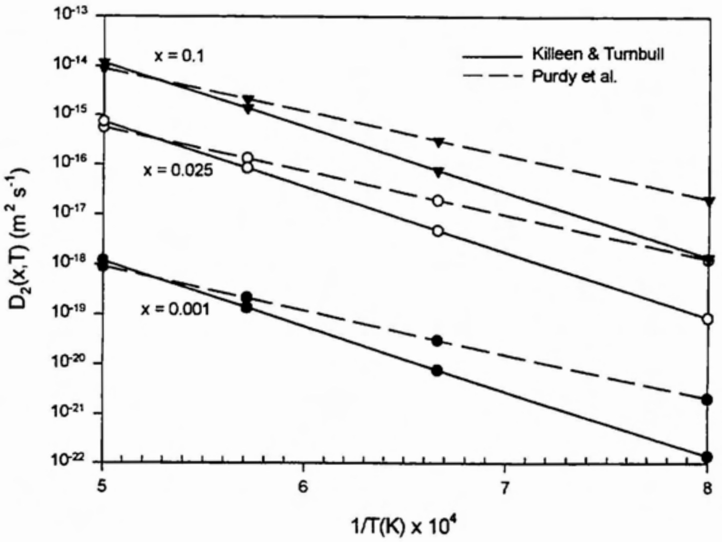

Figure 8. Comparison of the (out-of-pile) vacancy-enhanced diffusion component for non-stoichiometric fuel (Eq. (25)) as a function of stoichiometry deviation and temperature based on the Killeen and Turnbull, and Purdy et al., pre-exponential and activation constants.

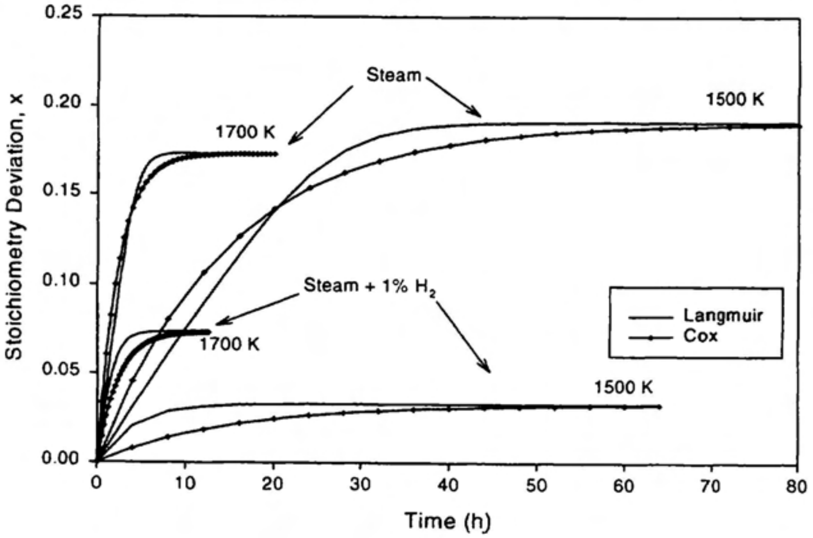

Figure 9. Comparison of the fuel oxidation kinetics at a pressure of 1 atm in a pure steam and steam-1%H_2 atmosphere at 100 and 1700 K. The fuel oxidation kinetics are based on a solution of the phenomenological model of Cox et al. in Eq. (27) and the Langmuir adsorption treatment of Eq. (28).

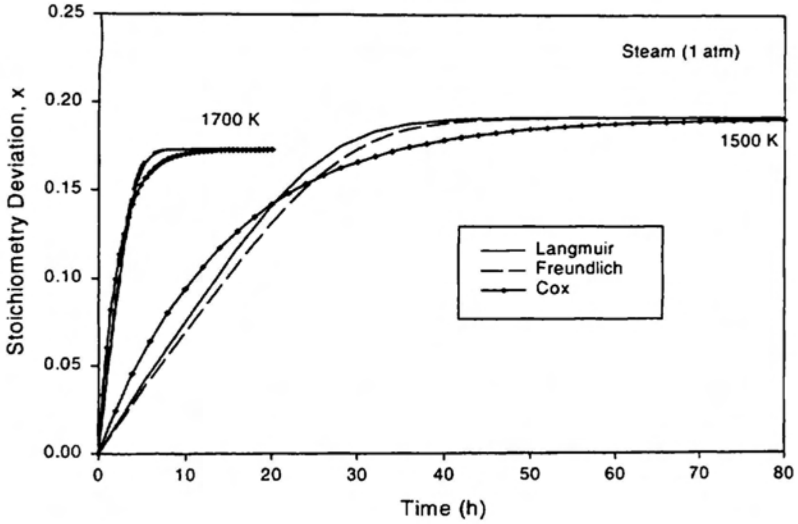

Figure 10 Comparison of the adsorption isotherm models (Langmuir and Freundlich) versus the phenomenological model of Cox et al. for fuel oxidation in pure steam at a pressure of 1 atm and temperatures of 1500 and 1700 K.

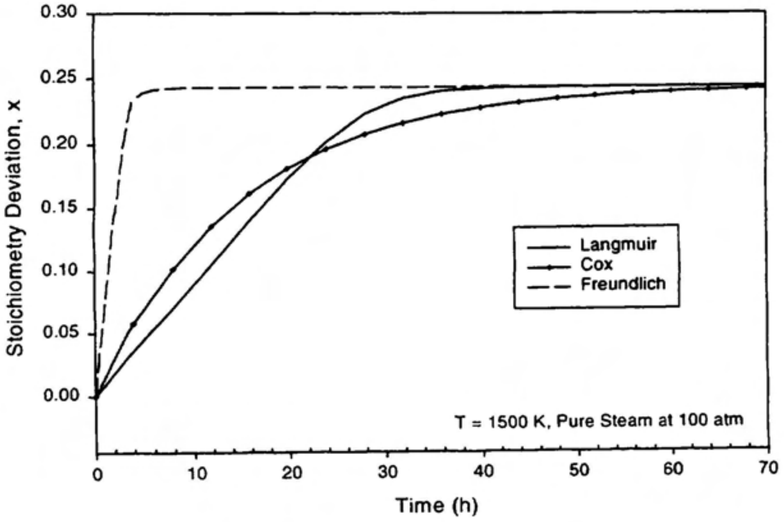

Figure 11. Comparison of the adsorption isotherm models (Langmuir and Freundlich) versus the phenomenological model of Cox et al. for fuel oxidation in pure steam at a high pressure of 100 atm and temperature of 1500 K.

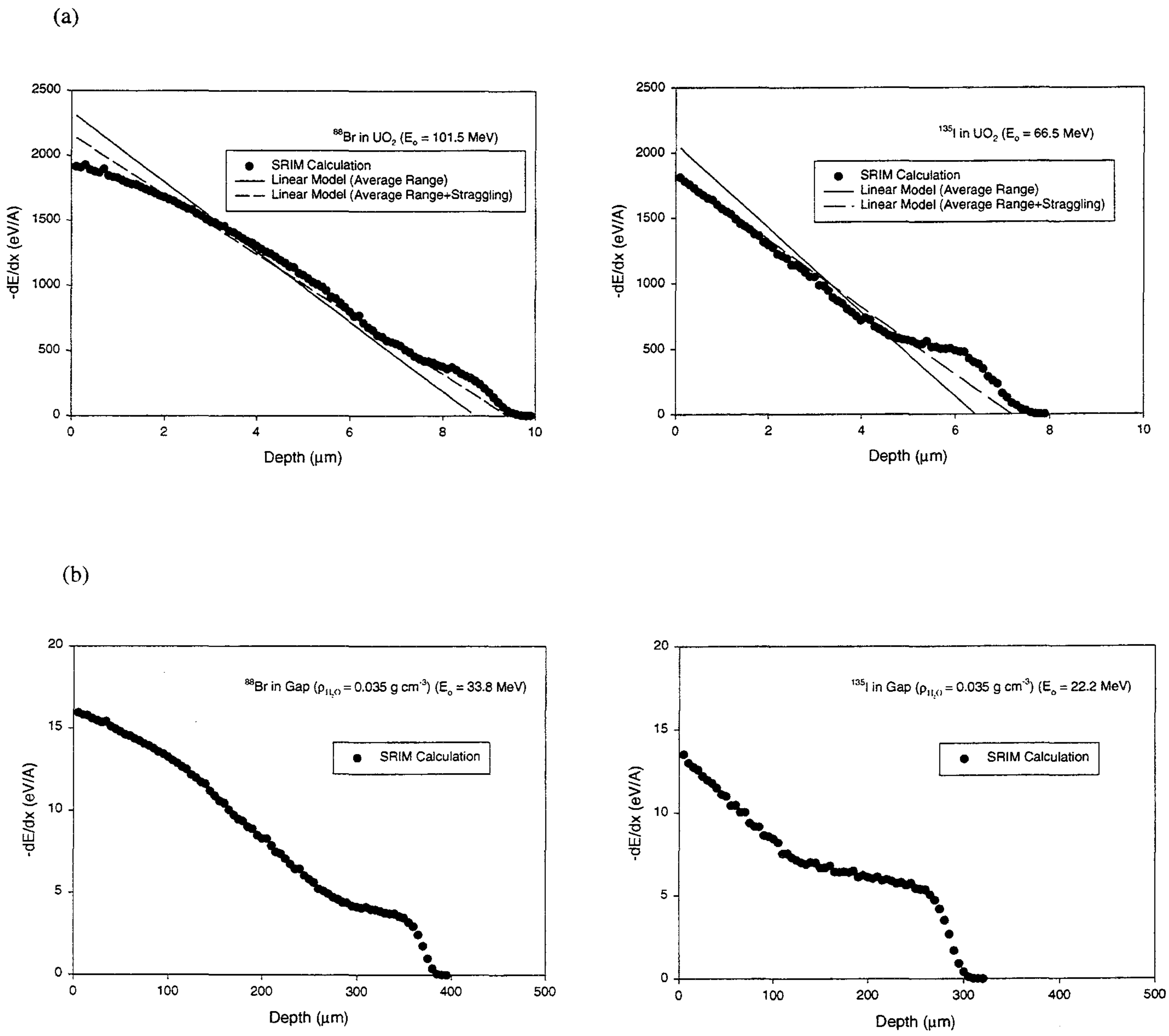

Figure 12. Energy loss of fission fragments ^{88}Br and ^{135}I in the (a) UO_2 fuel and (b) steam-filled fuel-to-clad gap. A linear energy loss approximation for the slowing down of the fission fragments in the UO_2 is also shown.

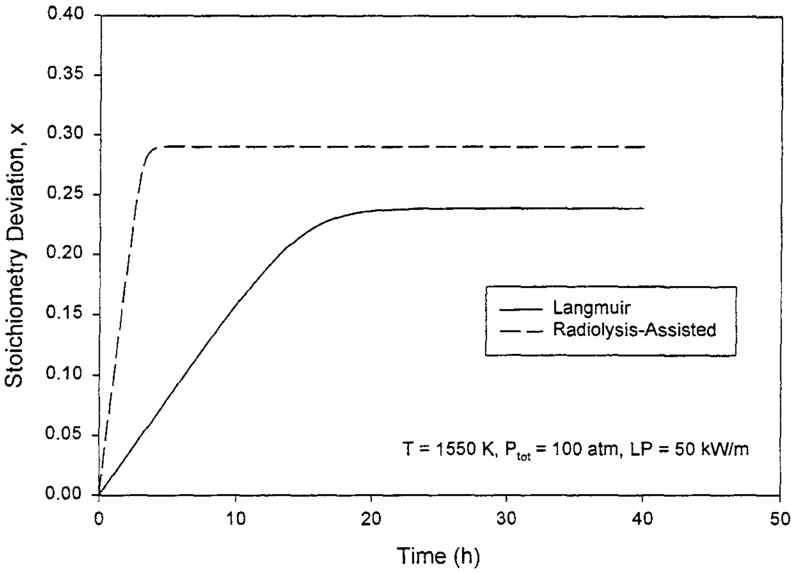

Figure 13. Comparison of the fuel oxidation kinetics with and without radiolysis-assisted oxidation.

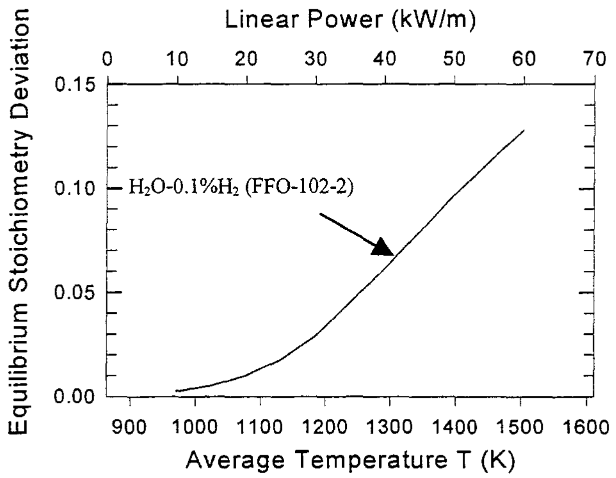

Figure 14. Prediction of the equilibrium stoichiometry deviation x_e as a function of the fuel rod linear power and average fuel temperature. The calculation assumes a high pressure of 100 atm and a partial pressure ratio of hydrogen-to-steam of 0.1%.